



ELSEVIER

Available online at www.sciencedirect.com

SCIENCE @ DIRECT®

Journal of Constructional Steel Research 61 (2005) 1576–1593

JOURNAL OF
CONSTRUCTIONAL
STEEL RESEARCH

www.elsevier.com/locate/jcsr

Development and validation of a numerical model for buckling of coped beams

J. Maljaars^{a,b,*}, J.W.B. Stark^c, H.M.G.M. Steenbergen^b,
R. Abspoel^c

^a*Eindhoven University of Technology, Faculty of Architecture, Building and Planning, 5600 MB Eindhoven,
The Netherlands*

^b*TNO Built Environment and Geosciences, 2600 AA Delft, The Netherlands*

^c*Delft University of Technology, Faculty of Civil Engineering and Geosciences, 2600 AA Delft, The Netherlands*

Received 31 March 2003; accepted 29 April 2005

Abstract

The lateral torsional buckling resistance of a beam depends on the support conditions. In structures for buildings, coped beams are often used. A numerical model is developed to investigate the influence of copes on the lateral buckling resistance. The model was verified with laboratory tests. This paper describes the background of the numerical model, the test program and the results of the validation. In a companion paper [Maljaars J, Stark JWB, Steenbergen HMGM, Abspoel R. Lateral-torsional buckling resistance of coped beams. *Journal of Constructional Steel Research* 2005;61(11):1559–75], the results of a parameter study are presented.

© 2005 Elsevier Ltd. All rights reserved.

Keywords: Lateral-torsional buckling; Building structures; Cope; Connection

1. Introduction

In some beam-to-beam connections, a part of the web and upper flange of the secondary beam is removed in order to level the upper sides of the main and secondary beam. The secondary beam is then called a coped beam and the removed part is called a cope.

* Corresponding author at: Eindhoven University of Technology, Faculty of Architecture, Building and Planning, The Netherlands. Tel.: +31 15 2763464.

E-mail address: johan.maljaars@tno.nl (J. Maljaars).

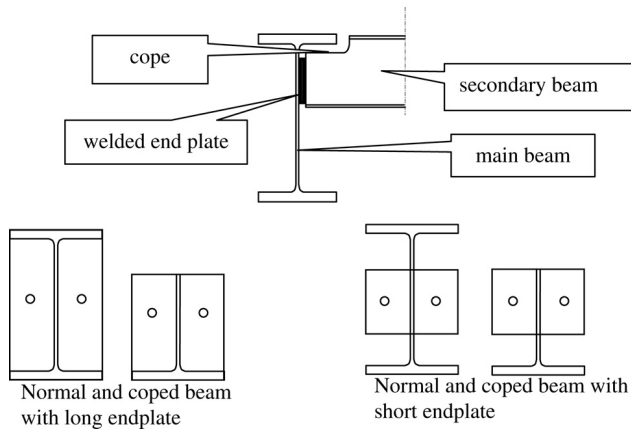


Fig. 1. Coped connections with long or short endplates.

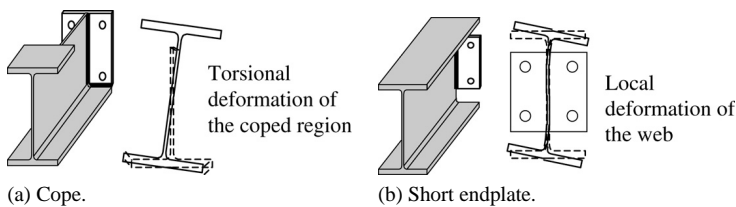


Fig. 2. Deformations in case of a cope or a short endplate (deformations are exaggerated).

This research concentrates on coped beams connected with endplates to the main beam. Distinction is made between endplates welded to the complete height of the beam end (long endplate) and endplates welded to a part of the web only, leaving the bottom flange unsupported (short endplate), Fig. 1.

Secondary beams supported by main beams are usually assumed to be simply supported, i.e. the rotation about the longitudinal axis is restrained but rotations about the strong and weak axes and warping are free to occur. This assumption is followed in the current research.

A beam loaded in bending about the strong axis is subjected to lateral–torsional buckling. A cope may adversely affect the lateral–torsional buckling stability of the beam due to greater torsional flexibility of the coped region (Fig. 2(a)). In addition, if short endplates are used, local deformation of the web may occur, causing the end of the section to rotate about the longitudinal axis (Fig. 2(b)). This may also result in reduction of the buckling load.

Codes for steel structures and handbooks on stability give verification methods for lateral–torsional buckling of beams with supports that prevent deformation of the web. Coped beams and beams with short endplates are usually not within the scope of these verification methods.

In the current study, a numerical model for coped I- or H-section beams was developed in the finite element program DIANA. The simulations carried out with this geometrically and physically nonlinear numerical model were checked with full-scale tests. This paper describes both the numerical model and the tests. It might be used as an example for studies on other stability problems. In a companion paper [1] the results of a parameter study are given together with design rules for use in practice.

2. Differences with other research projects

Buckling of coped beams has been the subject of many research projects. du Plessis [2], Lindner and Gietzelt [3], Cheng et al. [4], Lam et al. [5] and Abspoel and Stark [6,7] studied the elastic critical (Euler) buckling load of coped beams using a numerical model. Gupta [8] derived an analytical model by using assumed deformations to obtain approximate elastic critical buckling loads. From the results of the research projects it follows that copes reduce the elastic critical buckling load. This reduction, which is significant for large cope dimensions, large height over web thickness ratios and large height over span ratios, has been quantified in most of these research projects. The current research not only concentrated on the influence of the cope on the elastic critical buckling load, but also on the buckling resistance (including influences of plasticity, residual stresses, large displacements and initial geometric imperfections). For this purpose, a geometrical and physical nonlinear model was developed.

Numerical models used in the current research and those used in previous research projects consisted of shell elements. Because these elements do not have a volume, the geometric properties of the cross-section of the model do not perfectly correspond with the geometric properties of the real section. This difference is significant for the torsional constant, which is an important parameter for lateral torsional buckling. In the current study, the model was adapted in such a way that the geometric properties of the model corresponded better with the real geometric properties. This resulted in better determination of elastic critical buckling loads and resistances of real sections.

du Plessis [2], Cheng and Yura [9], and Lindner [10–14] carried out full-scale tests on coped beams for determination of the buckling resistance. These tests were carried out with connections to main beams as applied in practice, resulting in partial restraints to rotation about the weak and strong axes of the beam supports. Because the numerical model was developed for simply supported beams, the tests in the current research were also carried out with simple support conditions. Initial geometric imperfections were measured carefully, so that they could be introduced in the numerical models.

3. Description of tests

The tests in the current research were carried out in such a way that they approach pure lateral–torsional buckling. This resulted in the following requirements for the test set-up:

- The load should be conservative, i.e. it should follow the buckled beam while the work-line remains vertical and the application point on the beam does not change;
- Rotation of the endplates about the strong and weak axes and translation in longitudinal direction should be free to occur;

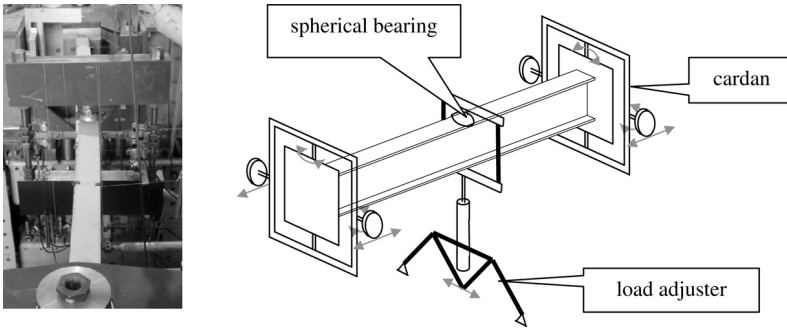


Fig. 3. Overview of test set-up.

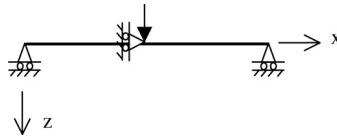


Fig. 4. Static system of the tests.

- At the supports translations in strong and weak directions and rotation about the longitudinal axis should be restrained;
- Friction in the load application and in the supports should be minimized to such an extent that the influence on lateral–torsional buckling is negligible.

Geometrical and physical properties of the test specimens were measured. The measured properties include:

- Dimensions of the cross-section;
- Material properties;
- Initial imperfections on the out-of-straightness and torsion of the beam;
- Initial imperfection on the load application point.

In this way, it is possible to simulate the tests as accurately as possible with numerical models.

Ten laterally unsupported standard European IPE120 beams with a span of 2 m and a concentrated load at midspan were tested. The test specimens include coped and uncoped beams with short and long endplates. Because of the relatively short span ($h/l \approx 1/17$) a significant influence of copes on the buckling resistance is to be expected. An overview of the test set-up is given in Fig. 3.

3.1. Support conditions

At midspan, the displacement in longitudinal direction was prevented by fixing the work-line of the load in the longitudinal direction. In order to prevent normal reaction forces, both supports are rolls. The static system is according to Fig. 4.

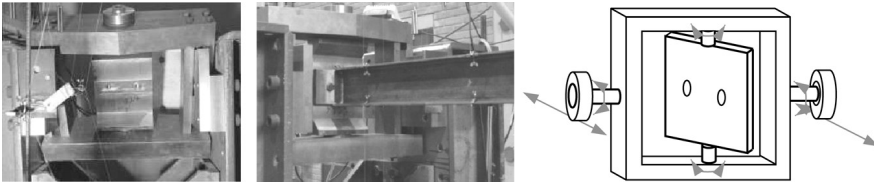


Fig. 5. Cardan support.

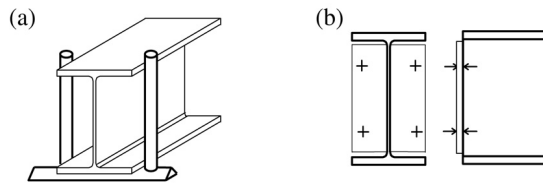


Fig. 6. End conditions of reference beams.

The endplates welded to the test beam were part of the test model. The structures that support these endplates, however, were part of the test set-up. For accurate testing, these structures have to support the endplates such that the endplates are restrained to rotation about the longitudinal axis and to lateral and vertical translations, but are free to rotate about the strong and weak axes (simple support conditions). A cardan construction with a horizontal and a vertical axis is developed to approach these support conditions (Fig. 5). The endplate was bolted to the central plate of this cardan.

Two beams were tested that were aimed to approach the behaviour of beams with a uniform cross-section along the span and with supports that prevent web deformation, but allow free warping. These support conditions are referred to as fork supports (Fig. 6(a)). In the set-up, fork conditions were approached by welding an endplate to the section that covers the web but not the flanges of the section (Fig. 6(b)). The endplates were not welded to the flanges, as this may introduce restraint to warping.

3.2. Load introduction

The beams were loaded by a concentrated load applied at midspan. The height of load application influences the elastic critical buckling load. Verification rules in codes for beams with uniform cross-sections are derived for load application in the section centroid and in the centres of the flanges. In this research, loads were applied in the centre of the upper flange.

An actuator introduced the load via a load adjuster. This load adjuster keeps the work-line of the load parallel to the original work-line in deformed shape of the beam (Fig. 7).

The load was transferred from the actuator to the specimen by a spherical bearing. The radius of this bearing determines the height of the load application, as illustrated in Fig. 8. Ideally this bearing should be frictionless but practically this could not be realized. Separate tests were carried out to determine the coefficient of friction. This coefficient turned out

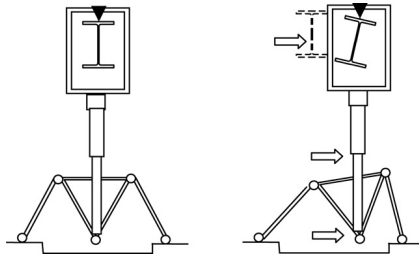


Fig. 7. Load introduction by an actuator and a load adjuster.



Fig. 8. Spherical bearing.

not to be constant, but varied in the tests. A coefficient of friction was measured ranging from 0.4% to 0.7%.

3.3. Geometry of the cross-section

At seven places along the span of each specimen, web and flange thickness, web height, root radii at the intersection between web and flanges, width of both flanges and the angles between web and flanges were measured. Also, cope depth, cope length, span and endplate position and height were measured.

3.4. Material properties

The yield strength and ultimate tensile strength of the web and the flanges were determined with coupon tests after the buckling tests were carried out. These coupon tests were taken from parts of the tested beams in which yielding was neither detected nor expected (Fig. 9). The yield strength and ultimate tensile strength were assumed to be constant along the span. The modulus of elasticity and Poisson ratio were not measured, but assumed to be $206\,000\text{ N/mm}^2$ and 0.3, respectively.

3.5. Initial imperfections

3.5.1. Residual stresses

Residual stresses potentially influence the buckling resistance; however, they are difficult to measure accurately. The influence of residual stresses on the buckling resistance of the specimen was determined in a numerical sensitivity analysis. For this purpose, buckling resistances were determined for all beams in the test program with an assumed

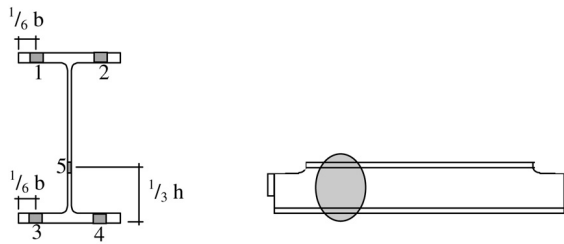


Fig. 9. Places where the yield strength was determined.

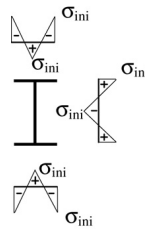


Fig. 10. Residual normal stresses applied in the numerical model.

residual stress pattern according to Fig. 10. This residual stress pattern is according to the Dutch code NEN 6771 [15]. The maximum initial stress (σ_{ini}) was varied as 27%, 30% and 33% of the yield strength. This variation in maximum initial stress resulted in less than 0.5% variation in the buckling resistance. This indicates that the sensitivity to variations in residual stresses for the beams considered was small.

The actual residual stresses of the specimens were not measured. Instead, the residual stress pattern according to Fig. 10, with a maximum initial stress (σ_{ini}) equal to 30% of the yield stress, was applied.

3.5.2. Initial geometric imperfections

For measuring the out-of-straightness imperfections, a special reference beam was fabricated. This reference beam had seven cross-sections with nominal dimensions along its span, positioned exactly straight in between the beam-ends. This reference beam was produced by taking a rolled beam and welding extra material at the seven cross-sections. The beam was subsequently milled to nominal dimensions.

Lateral and vertical positions and angle about the longitudinal axis of the seven cross-sections of all specimens were measured in relation to this straight reference beam (Fig. 11).

4. Description of numerical models

Numerical models were developed for the tested beams described in Section 3. With these numerical models, the tests were simulated.

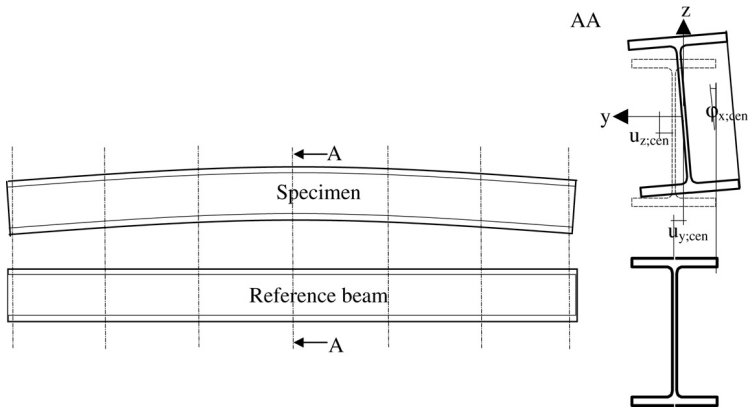


Fig. 11. Measuring initial geometric imperfections by comparison with a straight beam (not on scale).

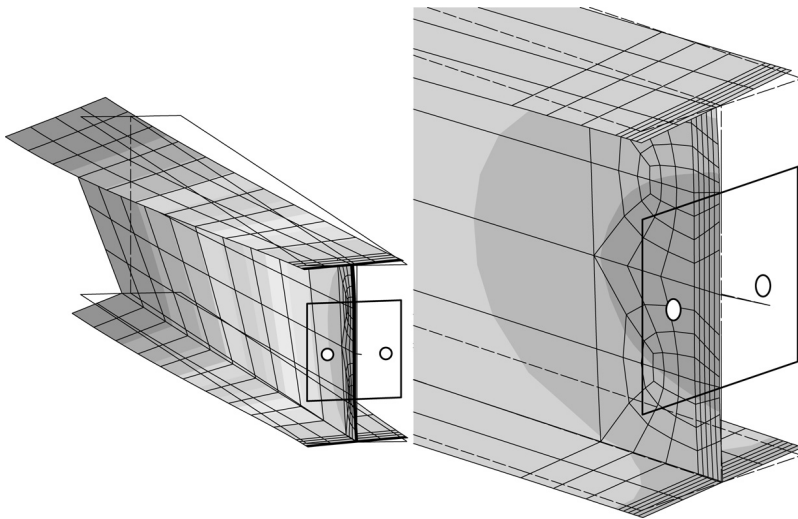


Fig. 12. Model with short endplate (half girder, deformations are exaggerated).

Fig. 12 gives the deformed shape of a simulation of a half beam with short endplates. Fig. 13 gives the deformed shape of a simulation of a half coped beam with short endplates. It should be noted that the endplates were not modelled as shown, but are displayed in the figures for reference. Different greyscales in the figures indicate the rotation about the longitudinal axis of the beam.

It is shown that the deformations in the simulation of a short, coped beam concentrate in the coped region, while deformations of the simulation of a specimen with endplates occur in the entire beam. For both types of beam, the largest local distortions of the mesh occur in the web at the edges of the endplates. At these locations a denser mesh was applied.

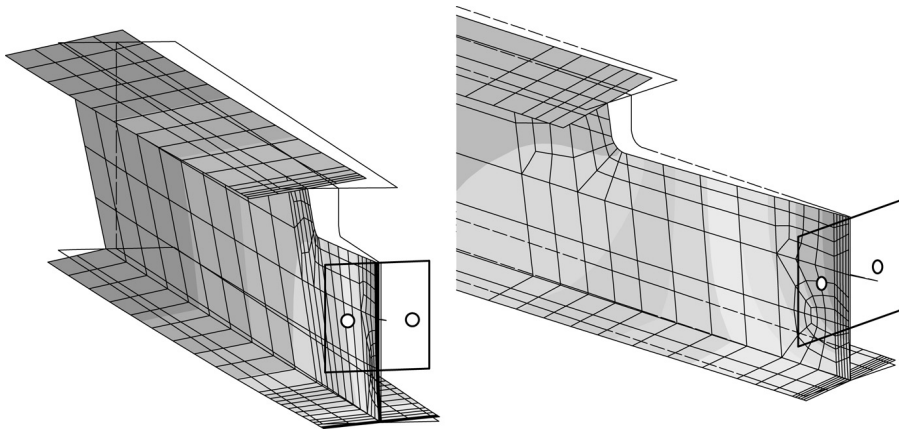


Fig. 13. Model with cope and short endplate (half girder, deformations are exaggerated).

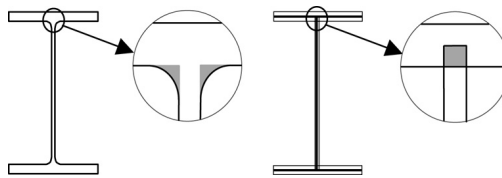


Fig. 14. Geometry of the cross-section of a real section (left-hand) and model with shell elements (right-hand).

4.1. Elements

For the numerical models eight-node shell elements were used to represent the web and the flanges. As shell elements do not have a volume, the section roots at the intersection between web and flanges could not be modelled exactly (Fig. 14). This results in a difference in cross-sectional properties between the real section and the numerical model. This difference is particularly significant in case of the torsional constant, which may be up to 30% for standard European IPE sections. Less significant differences in the torsional constant occur at the flange tips, where end effects are not taken into account in the numerical model.

In order to model the cross-sectional properties more properly, extra elements were added to the model in the intersection of web and flange. The extra beam elements were given such geometric properties that the geometric properties of the real section corresponded to that of the model. End effects at the flange tips were thus modelled by beam elements in the section roots. It was expected that this simplification does not significantly influence the buckling load.

The addition of elastic beam elements resulted in elastic critical buckling loads that correspond to the theory for lateral–torsional buckling of a simply supported beam loaded by a uniform moment. However, nonlinear analyses resulted in numerical instability and

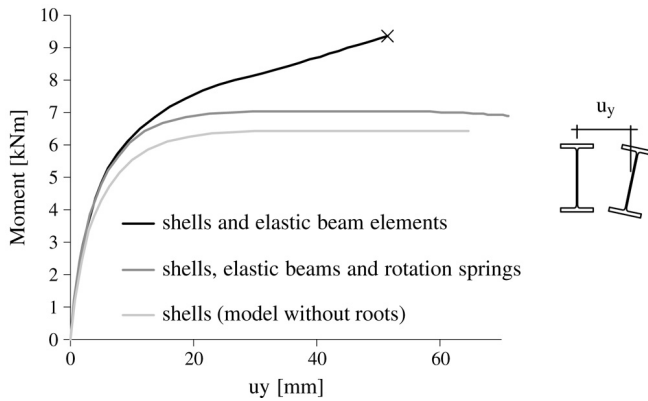


Fig. 15. Influence of modelling of the specimen roots on buckling.

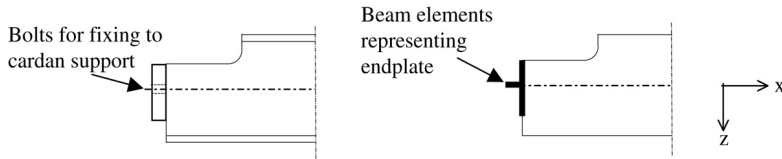


Fig. 16. Endplates in tests (left-hand panel) and numerical modelling (right-hand panel).

an unexpected relation between the load and the lateral displacement, when compared to a model without roots (Fig. 15). This is caused by the absence of a plastic range for torsion of the elastic beam elements. Therefore, the torsional properties of the section roots minus end effects at the flanges were represented in the model by rotation spring elements with an elastic stiffness and a plastic limit. A model consisting of shell elements for web and flanges, rotation springs for torsional properties of the roots and elastic beam elements for other properties of the roots results in buckling behaviour that corresponds well with a model without roots (Fig. 15).

4.2. Support conditions

In Section 3.1 it is explained that the endplates are part of the specimen. They are therefore also implemented in the numerical model. The endplates are represented by elastic beam elements along the web and, in case of long endplates, also along the lower flange. A beam element in the longitudinal direction represents the endplate thickness (Figs. 16 and 17).

The following stiffness properties are given to the beam elements:

- The torsional constant and the bending stiffness of the beam element along the web were taken equal to the stiffness to torsion, respectively the stiffness to bending, of the endplate. The endplate is so stiff for shear deformation that it functions as a full restraint

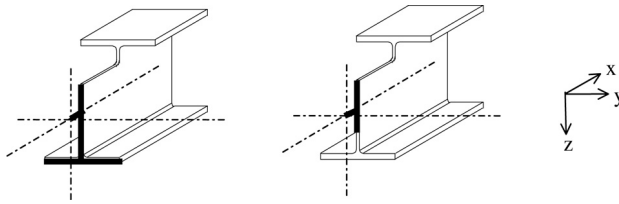


Fig. 17. Long end plate (left-hand panel) and short end plate (right-hand panel).

to in-plane deformation. The exact value of the bending stiffness for bending about the x -axis is therefore not important. This bending stiffness was taken equal to 10^7 mm^4 .

- The flanges are relatively stiff, so deformation of the ends of the flanges was not detected. The bending stiffness about the z -axis of the beam element along the flange, to represent a long endplate, is therefore not important and is taken equal to $5 \times 10^4 \text{ mm}^4$. The same arbitrary value was used for the torsional constant of this beam element. For bending about the x -axis of the flanges, the endplate is so stiff that it functions as a full restraint. The exact value of the bending stiffness for bending about the x -axis is therefore not important. This bending stiffness was taken equal to 10^7 mm^4 .
- The beam element in x -direction representing the endplate thickness should be so stiff to bending in all directions that it does not deform. The bending stiffness in both directions of this beam element was taken equal to $5 \times 10^8 \text{ mm}^4$; the torsional constant was $5 \times 10^7 \text{ mm}^4$. The end of this beam element is restrained against translations in strong and weak directions and rotation about the longitudinal axis, in order to model simple support conditions.

4.3. Geometry

The dimensions of the cross-section of the specimens varied only marginally along the span but differed significantly from nominal dimensions and between specimens. Therefore, the average values of the dimensions along the span as measured for each specimen were used in the numerical model of each beam.

Initial geometric imperfections and pre-buckling deflections influence the buckling resistance of a beam. In geometrically nonlinear analyses with the numerical model, the influence of these imperfections and deflections is implicitly taken into account.

The initial shapes of the test beams, and therefore also the buckling modes, were not symmetrical about midspan. Therefore, the total beam should be modelled. However, in simulations it was found that the place of the amplitude of the initial imperfection had no significant influence on the buckling resistance. Beams with different initial imperfections as shown in Fig. 18 thus have approximately equal buckling resistances if the amplitudes of these imperfections are equal. On this basis it was possible to model a symmetrical imperfection. As the first elastic critical buckling mode is in this case also symmetric and the magnitudes of the second and higher elastic critical buckling loads are much higher than the first, it is possible to model only half a beam (Fig. 19). This has the advantage that it saves calculation time in the parameter study.

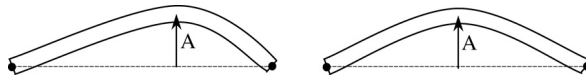


Fig. 18. Beams with different locations of the amplitude of the initial geometrical imperfection.



Fig. 19. Model of a half beam.

At midspan, boundary conditions for symmetry are applied, i.e. translation in the longitudinal direction and rotations about the weak and strong axes were restrained of all nodes in the cross-section at midspan.

4.4. Material properties

The material properties as given in Section 3.4 were applied in the numerical models. The entire stress–strain relation, including strain hardening, was modelled. As stated in Section 3.5, the residual stresses were not measured. The residual stress pattern according to Fig. 10 with a maximum equal to $\sigma_{\text{ini}} = 0.3 \times 235 \text{ N/mm}^2$ was applied.

5. Validation of the numerical model and comparison with the tests

The numerical models were validated in four steps. First, deformations of the coped region and the elastic critical buckling load of a prismatic beam were compared with analytical solutions. Second, the buckling resistances of prismatic beams determined with the numerical model were checked with the buckling resistances according to the European code for steel structures, EN 1993-1-1 [16]. Third, the results were checked with the outcomes of other numerical models. The final step consisted of a comparison with the tests. The steps are explained in the following sections.

5.1. Step 1: Validation with analytical models

The elastic critical buckling load for a girder in bending was analytically derived for a simply supported prismatic beam loaded by a uniform moment (Fig. 20). Three models of such beams were made: one of a stocky beam for which restrained warping is dominant for lateral–torsional buckling resistance, one of a slender beam for which torsion is dominant, and one of a beam for which the contribution of torsion and restrained warping to the lateral–torsional buckling resistance are approximately equal.

The elastic critical buckling load of the stocky beam determined with the finite element model was 2.1% lower than the elastic critical buckling load according to the analytical solution, among others given by Timoshenko and Gere [17]. The difference in the case of the other beams was lower. The difference between the analytical solution and numerical results is possibly caused by local deformations at places with a negative normal stress. This is taken into account in the DIANA calculation, but not in the analytical model.

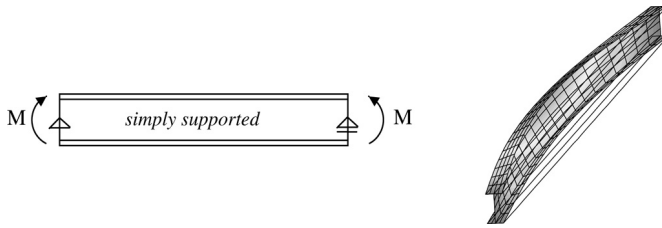


Fig. 20. First validation step: uniform moment.

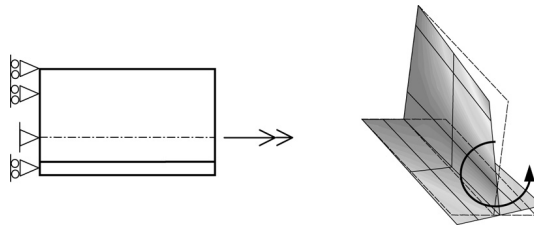


Fig. 21. First validation step: T-section.

Additionally a short T-section, representing the cope region, is loaded in torsion (Fig. 21). The finite element calculation resulted in a rotation that is 0.8% lower than the rotation according to the analytical solution.

From the results of the first validation step it was concluded that warping and torsion were sufficient accurately described in the finite element model, and that simple supports were modelled properly.

5.2. Step 2: Buckling resistance compared to the code

The European code that gives general rules for steel structures, EN 1993-1-1 [16], gives a method to determine the ultimate buckling resistance. Buckling curves are given which give the relation between the ratio of the ultimate buckling resistance ($M_{b,Rd}$) divided by the capacity of the cross-section ($W_y \cdot f_y$) and the square root of the ratio between the capacity of the cross-section ($W_y \cdot f_y$) and the elastic critical buckling load (M_{cr}), Fig. 22. Pre-buckling deflections are not taken into account in the determination of the elastic critical buckling load. The curves take into account the influence of geometric imperfections and residual stresses on the ultimate buckling resistance. The code specifies that curve ‘a’ should be applied for rolled sections with beam depth/width ratios smaller than or equal to 2 and that curve ‘b’ should be applied for rolled sections with beam depth/width ratios larger than 2. IPE 160 sections are in the first category, so curve ‘a’ should be applied for these sections, while curve ‘b’ should be applied for IPE 500 sections. It is noted that these design curves in the code are approximations by nature.

Numerical models are made of prismatic IPE 160 and 500 beams with various spans, loaded by a uniformly distributed load at midspan. The dots in Fig. 21 represent the results of analyses with these numerical models. It is shown that the numerically determined

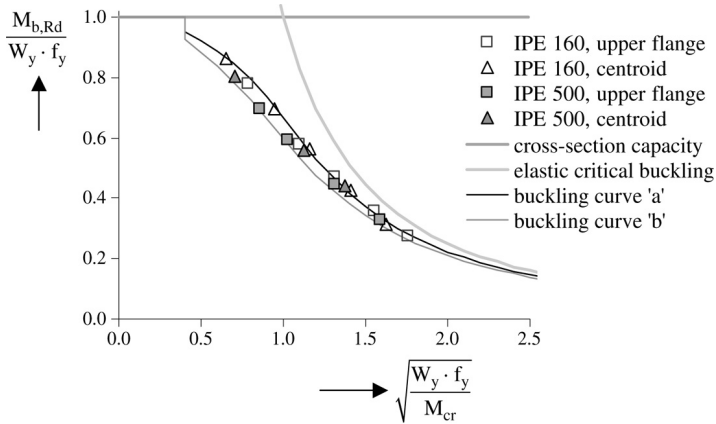


Fig. 22. Relation between M_{cr} , $W_y \cdot f_y$ and $M_{b,Rd}$.

resistances of IPE 160 beams correspond to buckling curve ‘a’, and that the resistances of IPE 500 beams correspond to buckling curve ‘b’.

5.3. Step 3: Comparison with results of other numerical models

For the third validation step, two different numerical models were selected:

- (1) The results of the models in the current study were compared to the buckling resistances determined by Greiner et al. [18]. Results were compared for a relatively slender and a relatively stocky beam loaded by a constant moment, a uniformly distributed load, and a concentrated load at mid-span. In all cases, the elastic critical buckling loads obtained by the models were equal. In case of constant moment, the lateral–torsional buckling resistance is equal as well. However, in case of loading by a concentrated load or a uniformly distributed load, the model used in this study resulted in a resistance up to 10% and up to 6% lower than given in Greiner. These differences are attributed to the use of other elements in the models. Loading by a uniformly distributed load or a concentrated load results in shear stresses and shear deformations. Local (web) deformations can be larger than in case of a constant moment loading. These effects are taken into account in the models used in the current research, but possibly not in the elements used in the models in Greiner. A coped beam has no uniform cross-section along its span and it is therefore not possible to model a coped beam with the elements used by Greiner.
- (2) For further verification, a second model was developed in the current research, consisting of solid elements. Results were again compared for a relatively slender and a relatively stocky beam loaded by a constant moment, a uniformly distributed load, and a concentrated load at mid-span. The differences between the shell element models and the solid element models were small: 0.5% difference in the critical elastic buckling load and 2.2% difference in buckling resistance.

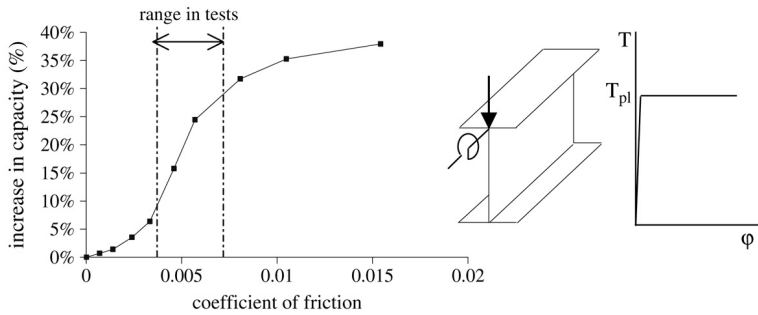


Fig. 23. Relation between increase in resistance and friction for beam A4.

5.4. Step 4: Comparison with tests

The buckling resistances of the tests described in Section 3 were compared to the numerically determined buckling resistances. As stated in Section 3, it was not possible to produce a bearing without friction for the load application in the tests. The coefficient of friction of this bearing was measured in separate tests. This coefficient of friction varied between the tests and ranged from 0.4% to 0.7%.









To determine the influence of this friction on the buckling resistance, a numerical sensitivity analysis was carried out for one of the beams (A4). Friction in the bearing was taken into account in the numerical model by adding a rotation spring element in the longitudinal direction to the node in which the load was applied. The rotation spring element had a high elastic stiffness and a plastic level that was varied. In Fig. 23 the relation is given between the coefficient of friction (plastic level of the rotation spring) and the ultimate buckling resistance of the beam.

The influence of friction on the ultimate buckling resistance is evident and cannot be neglected in the validation.

The measured resistances in the tests are compared to the numerically determined resistances in Table 1. The end conditions of the beams are indicated in the first and second columns of the table. The numerically determined slenderness (λ_{LT}) of the beams is listed in the third column. This slenderness is the root of the (numerically determined) capacity of the cross-section divided by the elastic critical buckling load. The fourth column gives buckling resistances determined in the tests (F_{test}). The numerically determined resistances (F_{num}) with friction magnitude equal to the maximum and minimum values of the measured friction are listed in columns five and six, respectively. The relation in Fig. 22 was used to determine these resistances. Using this relation, it is also possible to determine the coefficient of friction, for which the numerically determined capacity is equal to the measured capacity in the tests. This value of the coefficient of friction (Cf_{num}) is given in the seventh column.

The values of the coefficient of friction in column seven are within the measured bandwidth of the measurements on this coefficient of friction. Only for beam B1, the coefficient of friction in column seven is slightly higher than the range of friction measured.

Table 1
Buckling loads of the tests

Beam number	Connection	λ_{LT}	F_{test} (kN)	F_{num} ($C_f = 0.004$) (kN)	F_{num} ($C_f = 0.007$) (kN)	$C_{f_{num}}$
A1 (fork support) ^a		0.95	34.3	a		
A2 (fork support)		0.95	35.7	35.0	40.4	0.0043
A3 (90 mm endplate)		0.96	34.1	32.6	37.6	0.0047
A4 (60 mm endplate)		1.15	36.2	31.3	36.2	0.0070
B1 (coped, long endplate)		0.92	31.2	26.0	30.0	0.0092
B2 (coped, long endplate)		0.95	28.4	27.0	31.2	0.0047
B3 (coped, short endplate) ^b		0.99	b	26.0		
B4 (coped, short endplate)		0.96	25.1	23.4	27.1	0.0050

^a Imperfections of this beam were not measured correctly, so no numerical model was made.

^b This test failed because of problems with load introduction.

This is possibly caused by inaccurate measurements during the tests, or in the geometric or material properties.

However, the bandwidth of this friction results in a considerable dispersion of capacities. This comparison with tests thus provides an indication that the numerical models give accurate resistances. An exact validation was not possible.

6. Conclusions and recommendations

Tests carried out and simulations with numerical models confirm that the ultimate buckling resistance is reduced when copes are applied.

Apart from load introduction by the spherical bearing, the developed test set-up is suited to studying lateral–torsional buckling of beams with various connections.

Because of friction in this spherical bearing, exact validation of the numerical models by the tests was not possible. However, other validation steps carried out were satisfactory and it is therefore expected that lateral–torsional buckling of I- and T-sections is described properly by the developed numerical model.

A relatively small lateral support by friction of the load introduction causes a relatively high increase in resistance. Loads applied in practice normally give much more support to the beam than the spherical bearing used in this research. Beams with these load conditions might therefore have a considerably higher resistance than the design resistance according to codes.

Based on the results of this research project, the following recommendations for future research are given:

- To develop load introduction systems that cause less friction than the spherical bearing used. For example, a knife or pin support may introduce less friction. With this new load introduction system, beam spans other than 2 m should be tested.
- To apply four concentrated loads at a representative range of beams in order to simulate a uniformly distributed load.
- To study lateral support of loads applied in practice and the effect of such supports on the beam resistance.

References

- [1] Maljaars J, Stark JWB, Steenbergen HMGM, Abspoel R. Lateral–torsional buckling resistance of coped beams. *Journal of Constructional Steel Research* 2005;61(11):1559–75.
- [2] du Plessis DP. Lateral–torsional buckling of end notched steel beams. In: *Proceedings, international colloquium on stability of structures under static and dynamic loads*. Washington (DC): ASCE; 1977.
- [3] Lindner J, Gietzelt R. Zur Tragfähigkeit ausgeklinkter Träger. *Stahlbau*; 1985.
- [4] Cheng JJR, Yura JA, Johnson CP. Lateral buckling of coped steel beams. *Journal of Structural Engineering, ASCE* 1988;114(1):1–15.
- [5] Lam CC, Yam MCH, Iu VP, Cheng JJR. Design for lateral–torsional buckling of coped I-beams. *Journal of Constructional Steel Research* 2000;54:423–43. Elsevier.
- [6] Abspoel R, Stark JWB. Elastic lateral buckling of coped beams. In: *Proceedings of Eurosteel 1999*. Elsevier; 1999.
- [7] Abspoel R, Stark JWB. Elastic lateral buckling of coped beams. In: *Stability and ductility of steel structures, proceedings of the 6th international colloquium 1999*. Elsevier; 1999.
- [8] Gupta AK. Buckling of coped steel beams. *Journal of Structural Engineering, ASCE* 1984;110(9):1977–87.
- [9] Cheng JJR, Yura JA. Lateral buckling test on coped steel beams. *Journal of Structural Engineering, ASCE* 1988;114(1):16–30.
- [10] Lindner J. Influence of constructional details on the load carrying capacity of beams. *Engineering Structures* 1996;18(10):752–8.
- [11] Lindner J. Influence of structural connecting details on the load carrying capacity of beams. In: *Internationale Vereinigung für Brückenbau und Hochbau, 13th congress Helsinki*. 1988.
- [12] Lindner J, Gietzelt R. Biegedrillknicklasten von Walzprofilen IPE200 und IPE160 mit angeschweißten Kopfplatten und baupraktischen Ausklinkungen an den Trägerenden. *Vr 2042*, Technische Universität Berlin; 1982.
- [13] Lindner J. Einfluss von Quer-einspannungen auf die Gabellagerung. *Vr 2065*, Technische Universität Berlin; 1987.
- [14] Lindner J. Biegedrillknickuntersuchungen an ausgeklinkten Trägern unter Berücksichtigung der Quereinspannung. *Vr 2073*, Technische Universität Berlin; 1985.
- [15] NEN 6771. TGB 1990 Staalconstructies. *Stabiliteit*; 2000.

- [16] EN 1993-1-1. Eurocode 3: Design of steel structures — part 1-1: General rules and rules for buildings. 2004.
- [17] Timoshenko SP, Gere JM. Theory of elastic stability. 2nd ed. McGraw-Hill Book Company; 1961.
- [18] Greiner R, Salzgeber G, Ofner R. New lateral–torsional buckling curves κ_{LT} — numerical simulations and design formulae. ECCS TC 8 — Report 30th June 2000.